Geophysical Research Letters

RESEARCH LETTER
10.1029/2020GL086957

# The Influence of Sea Surface Temperature Reemergence on Marine Stratiform Cloud

**Andrew Geiss**[1], **Roger Marchand**[1], **and LuAnne Thompson**[2]

[1]Department of Atmospheric Sciences, University of Washington, Seattle, WA, USA, [2]School of Oceanography, University of Washington, Seattle, WA, USA

**Key Points:**
- Global patterns of SST reemergence and of cloud-SST interaction are examined
- One region in the northeastern Pacific is identified where wintertime low cloud occurrence is correlated with the previous winter's SST

**Supporting Information:**
- Supporting Information S1

**Correspondence to:**
A. Geiss,
avgeiss@gmail.com

**Citation:**
Geiss, A., Marchand, R., & Thompson, L. A. (2020). The Influence of Sea Surface Temperature Reemergence on Marine Stratiform Cloud. *Geophysical Research Letters*, *47*, e2020GL086957. https://doi.org/10.1029/2020GL086957

Received 14 JUN 2019
Accepted 14 FEB 2020
Accepted article online 18 FEB 2020

**Abstract** The global distribution of winter to winter sea surface temperature (SST) reemergence is analyzed using a novel metric based on an autoregressive 1 model, and the global impact of SST on cloud amount and cloud type are examined using satellite data. A region in the northeastern Pacific Ocean is identified where wintertime SSTs are correlated with the occurrence of marine stratiform cloud the following winter. This correlation is likely a manifestation of SST reemergence. We hypothesize that through this reemergence mechanism marine stratus cloud amount, and thus shortwave cloud radiative effect, in the northeastern Pacific exhibits memory on inter-seasonal and even multi-year time scales and that exploration of this relationship may provide insight into the SST—low cloud feedbacks.

**Plain Language Summary** Global satellite records of ocean temperature and cloudiness are compared, and one region in the North Pacific Ocean is identified where wintertime cloud amount is related to sea surface temperature from the prior winter. This is due to a combination of two well-established effects: the strong link between low clouds and sea surface temperature, and sea surface temperature reemergence, a tendency for wintertime ocean temperatures to be influenced by ocean temperature from the previous winter. This relationship may be useful for understanding how cloud and sea surface temperature might interact in a changing climate.

## 1. Introduction

Midlatitude sea surface temperatures (SST) exhibit memory between successive winter seasons. This "SST reemergence" (Alexander & Deser, 1995; Alexander et al., 2001) results from the seasonal cycle of midlatitude mixed layer depth and was first suggested by Namias and Born (1970, 1974). In winter, ocean temperature anomalies are constant from the surface through the deep wintertime mixed layer and are sequestered beneath the seasonal thermocline and shallow mixed layers that form in late spring and early summer owing to surface heating and reduced wind stress (Kara et al., 2003). The mixed layer then deepens and entrains the sequestered water during the following fall and winter, allowing the previous winter SST anomaly (SSTA) to influence the current SST. SSTA reemergence occurs over much of the extratropical oceans, and more recent studies have explored the spatial distribution and timescales of this phenomenon using observations: Timlin et al. (2002) identify regions of reemergence in the Sargasso Sea and in the northeastern Atlantic, and Coëtlogon and Frankignoul (2003) find evidence of reemergence in most of the North Atlantic except for the central North Atlantic where there is strong subduction. Alexander et al. (1999) and Hanawa and Sugimoto (2004) find Pacific regions with reemergence signals on 8- to 12-month time scales. Finally, Zhao and Li (2010) find that a 12-month SSTA recurrence pattern dominates the North Atlantic and central North Pacific between 30°N and 50°N, while there is shorter winter to fall reemergence farther north. While the precise regions of SSTA recurrence identified by these studies may differ, owing to different criteria and methods, they agree that the SSTA reemergence mechanism is a prevalent feature of the midlatitude oceans.

Marine stratiform cloud (MSC) plays a critical role in the Earth's radiation budget, and there have been substantial and ongoing efforts to understand the thermodynamic and dynamical controls on MSC occurrence (McCoy et al., 2017; Bretherton, 2015; Zhang et al., 2009; Wood & Bretherton, 2006; Norris & Leovy, 1994; Hanson, 1991). Wood (2012) provides a comprehensive review of this topic. Persistent MSC occurs in the subtropical marine boundary layer in the eastern portions of the world's ocean basins: regions characterized by tropospheric subsidence, a strong capping inversion, and cool SST. Many observational studies have

compared marine low cloud amount and numerous physical variables, for example, tropospheric subsidence, estimated inversion strength (Wood & Bretherton, 2006), and SST. They have found that low cloud amount in these regions is reduced with warmer SSTAs (Peterson et al., 1992; Klein & Hartmann, 1993; Weare, 1993; Klein et al., 1994; Norris & Leovy, 1994; Clement et al., 2009; Eitzen et al., 2010; McCoy et al., 2017; Klein et al., 2010). Most of these studies derive observational estimates of the low cloud response to SST, based on the time correlation between MSC anomaly and SSTA, and some have estimated the low cloud radiative feedback driven by SST (e.g., Evan et al., 2012; Oreopoulos & Davies, 1993). While the magnitude of these estimates vary between studies, there is unanimous agreement in the sign and significance of these relationships. These studies show how low-level cloud might respond in a global warming scenario, a critical feedback which remains highly uncertain in climate modeling studies (Bony & Dufresne, 2005; Boucher et al., 2013).

To the best of our knowledge, while some have studied MSC-SST lag correlations (Klein et al., 1994; Norris & Leovy, 1994; Oreopoulos & Davies, 1993), no studies have examined lag correlations following specific seasons or time lags large enough to identify a relation between cloud and SSTA reemergence. Given the body of observational evidence suggesting winter-winter SSTA reemergence and SST controls on MSC amount, we now ask: Does wintertime or early spring SST influence low cloud amount the following winter? Furthermore, what implications might such a relationship have for regional cloud radiative effects and inter-seasonal and multi-year climate variability?

## 2. Data

Three data sets are used in this analysis. The first is NOAA's Optimum Interpolation Sea Surface Temperature data set (Reynolds et al., 2008). This product uses optimum interpolation to combine and grid SST observations from ships, buoys, and the Advanced Very High Resolution Radiometer satellite instrument (Banzon et al., 2016). Here, 5-degree gridded monthly means of SST from 1982 to 2015 are used. We use the "AVHRR-only" version of this data set, as the AMSR-E version ends in 2011.

The second is the Multiangle Imaging Spectroradiometer (MISR) L3 gridded monthly cloud top height and optical depth (CTH-OD) cloud fraction joint histogram data set (Version 6), from 2000 to 2015 (Marchand et al., 2010), averaged to a 5-degree grid. MISR orbits aboard EOS Terra and uses stereo-imaging to derive cloud top height (Diner et al., 1998). The joint histograms bin cloud fraction with respect to the retrieved cloud top height and optical depth (Marchand et al., 2010) and the cloud fraction within each bin represent how frequently cloud with that bin's CTH-OD properties is observed over a region during a given month.

Finally, the results obtained using MISR cloud observations are compared to similar 5-degree monthly joint histograms from the MODerate resolution Imaging Spectrometer (MODIS) on EOS Terra. The data used are MODIS Terra collection 6 global 1-degree gridded monthly CTP-OD (cloud top pressure and optical depth) cloud fraction joint histograms, from 2000 to 2015 (filename MOD08) (Hubanks et al., 2015). MODIS is a 36-band radiometer and retrieves cloud top pressure using infrared cloud top brightness temperature and $CO_2$ slicing techniques.

## 3. Method and Results

We break our analysis into three subsections. In the first, we develop an SST reemergence index using the OISST data set. In the second, we examine instantaneous regression coefficients between MISR monthly cloud occurrence and SSTA. Finally, we examine the relationship between low cloud cover and SST using lagged regression focused on the time scale and season where SST reemergence is strongest in each hemisphere.

### 3.1. A Sea Surface Temperature Anomaly Reemergence Index

Here we define a near global 5-degree gridded point-wise index of SSTA reemergence strength. SST reemergence is seasonally driven, so we examine "seasonal lag correlations" between a specific month of the year and specific successive months out to lags of 16 months. This results in a 12-start-month by 16-lag-month correlation matrix. Zhao and Li (2010) define regions of reemergence as locations where the SST seasonal autocorrelation function first drops below a threshold and then reaches a local maximum above the threshold at longer lag times. We instead examine deviations from the expected autocorrelation function of an

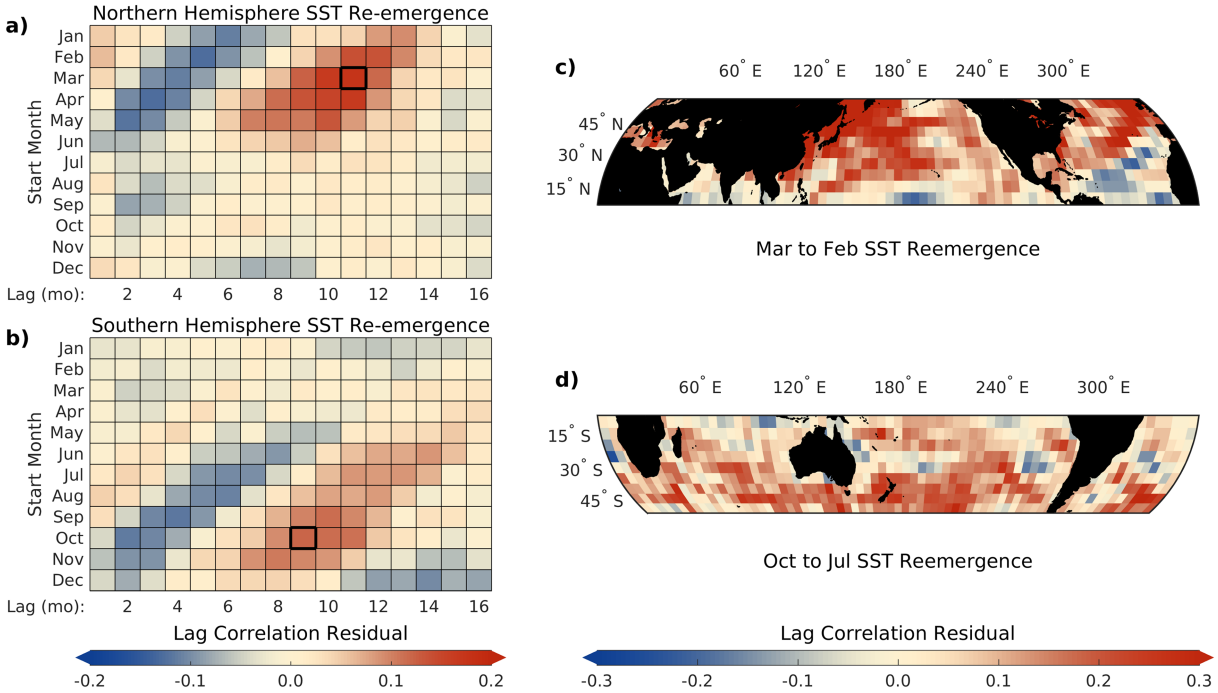


**Figure 1.** Global distribution of winter SST reemergence for 1982–2015 shown as the difference between the observed SST autocorrelation function minus the autocorrelation expected from a red-noise process (residual correlation). Panels (a) and (b) display northern (25 N to 65 N) and southern (−65 S to −25 S) hemisphere averaged reemergence, respectively. These are seasonal correlations for lags (horizontal axis) following specific start months (vertical axis). The positive values around 9- to 12-month lag are evidence of the reemergence mechanism. The reemergence is strongest following each hemisphere's spring, and the month and lag with the largest residual are boxed (thick black lines). Based on this, panel (c) shows the spatial distribution of March-February reemergence index in the northern hemisphere, and (d) shows the spatial distribution of October-July reemergence.

autoregressive-1 (AR1) process, also known as a red-noise or Markov process. For an AR1 process the current value depends on the value at a previous time step plus an instantaneous forcing. The autocorrelation function of the first order autoregressive processes is given by

$$r(\tau) = e^{-\frac{\tau}{T}} \tag{1}$$

(Von Storch & Zwiers, 2001, Equation (11.4), where their $\alpha_1 = e^{-\frac{1}{T}}$), where $\tau$ is the lag and $T$ is the correlation-length or the e-folding time scale (we find the global and seasonal average of $T$ is 4.2 months). The ocean mixed layer has "thermal inertia," so that monthly SST is dependent on the previous month's SST plus some external forcing due to ocean heat transport, ocean vertical mixing, air-sea turbulent heat fluxes, and surface radiative fluxes; so an AR1 model for SST is appropriate. Deviation of the observed autocorrelation from (1) provides a measure of SST reemergence strength, because a positive deviation implies that SST from earlier times than the previous month are influencing the present SST. Our approach then is to (1) compute lagged seasonal autocorrelation functions for detrended and deseasonalized SSTA for each 5-degree grid cell; (2) fit equation (1) to obtain a value for $T$ in each grid cell (see supporting information Section 1); and (3) take the difference, or residual, between observed SSTA autocorrelation and the fit at each lag. This difference is interpreted as an index for the strength of the reemergence.

Reemergence is such a dominant feature of extratropical SST variability that it can be seen in hemispheric means. Figure 1 shows our reemergence index averaged over the northern hemisphere from 25–65°N in panel (a) and 65–25°S in panel (b). The red areas in Figures 1a and 1b show seasonal SSTA autocorrelations that deviate above what is expected from a red-noise process 8–12 months following the winter/early spring. We examine the spatial distribution and dependence (Figures 1c and 1d) of winter-winter reemergence for the start-month and lag combination that show the largest positive values in Figures 1a and 1b (boxed bins). Reemergence is widespread in the northern hemisphere (Zhao & Li, 2010), though it is significantly stronger in some regions (Hanawa & Sugimoto, 2004; Timlin et al., 2002). We note that the SST autocorrelation

functions could deviate from that of a red-noise process for reasons other than the SST reemergence mechanism. For example, deviations might also be a result of memory in the atmospheric forcing, nonlocal effects (e.g., energy advection by ocean currents), or residuals in de-seasonalizing the data. The spatial distribution and timescales identified in Figure 1 are consistent with past work, however. The strongest reemergence signals occur at 11 months following March in the northern hemisphere and 9 months following October in the southern hemisphere, so our analysis below focuses on these timescales.

### 3.2. Instantaneous Sea Surface Temperature to Cloud Fraction Anomaly Comparison

Here we examine instantaneous relationships between SSTA and cloud fraction anomaly (CFA) by computing regression coefficients between the CFA in each bin in the MISR joint histograms and SSTA at each 5-degree grid point. This differs from past studies that have computed instantaneous regression coefficients between SSTA and low CFA only (e.g., Norris & Leovy, 1994; Oreopoulos & Davies, 1993). The mean, seasonal cycle, and any linear trend are subtracted from both data sets. While some past studies have used other predictors of marine cloud amount like estimated inversion strength (EIS) that is defined by atmospheric variables (Wood & Bretherton, 2006, here we are interested in the potential interaction between cloud fraction and seasonal changes in SST through the reemergence mechanism.

MISR only retrieves cloud optical depths over ice-free sun-lit ocean, so this analysis is limited to ocean regions equatorward of 57.5°N and 52.5°S. The regression coefficients represent the expected change in cloud fraction given a change in SST, in $\%K^{-1}$. We then perform a $k$-means clustering (using $k = 4$) on the regression coefficients (Bishop, 2006, p. 424), to identify regions that have a similar cloud-SST relationship with respect to cloud type (see supporting information Section 2 for details).

We find three clusters with strong SSTA-CFA linkages in the tropics and subtropics (clusters 2, 3, and 4, in Figure 2), while cluster 1 identifies regions (gray in Figure 2a) with no strong SST-CFA relationship and covers most of the high latitudes, where atmospheric synoptic variability likely dominates any SST influence on cloud occurrence. Cluster 2 (blue) only occurs in the tropics and mostly in areas well known for changes in cloud cover in response to El Niño Southern Oscillation (ENSO) (Marchand, 2013; Su & Jiang, 2013). The regression coefficients show a negative relationship between low cloud and SSTA and a positive relationship between mid- and high-altitude cloud and SSTA. MISR cannot observe low cloud underneath high cloud, and in Figure 2 we do not account for this. Assuming random overlap (Marchand, 2012) suggests that $-2.5\%$ of the $-5.6\%K^{-1}$ decrease in observed low cloud (CTH < 2.5 km) can be explained by occlusion from the $5.4\%K^{-1}$ increase high level cloud (CTH > 5 km) (estimated as $\Delta CF_{hi}{*}CF_{lo}/(1\text{-}CF_{hi})$). A reduction of low cloud in response to increased SST in the tropics is consistent with past studies (Wood, 2012).

Clusters 3 and 4 show relationships between subtropical cloud and SST. Cluster 4 (yellow in Figure 2a) is prominent in the eastern subtropical regions of each ocean basin. These regions are known for persistent MSC (Wood, 2012). Cluster 4 regression coefficients show that low-level marine cloud of moderate optical depth is negatively correlated with SSTA, in agreement with previous studies using satellite, ship, and buoy data (Hanson, 1991; Weare, 1993). Cluster 4 also shows some positive coefficients for clouds with $\tau < 1.3$. We speculate that as SST increases in this region, the inversion strength decreases, resulting in a higher and thicker boundary layer, and breakup of the MSC layer (Cesana et al., 2019; Wood, 2012). MISR and other satellite imagers typically overestimate the area covered by broken clouds and underestimate the optical depth (Marchand et al., 2010; Zhao & Di Girolamo, 2006), such that one might expect to see an increase of clouds with low optical depths, and perhaps slightly higher clouds, with a change in cloud morphology from stratocumulus to more broken, trade cumulus. Cluster 3 (red in Figure 2a) also shows negative SST-cloud fraction correlation for low cloud, but in this case the negative coefficients appear at higher CTH and lower optical depth ($0.3 < \tau < 3.6$). This relationship occurs west of the major subtropical stratocumulus regions, where low cloud cover is primarily trade cumulus. It is worth noting that regressions do not account for cloud advection and the possibility of nonlocal interactions. Clusters 3 and 4 both show a small increase in high cloud, and this may be due to a change in advection of tropical high cloud.

Summing over the regression coefficients for the low cloud bins (CTH < 2.5 km) in the joint histograms estimates the total response of low cloud to SST changes in the regions associated with each cluster. Cluster 2 gives $-5.59 \pm 0.17\%K^{-1}$; cluster 3, $-4.54 \pm 0.15\%K^{-1}$; and cluster 4, $-5.39 \pm 0.22\%K^{-1}$, where the intervals indicate 95% confidence. These values are consistent with past studies: Oreopoulos and Davies (1993) report

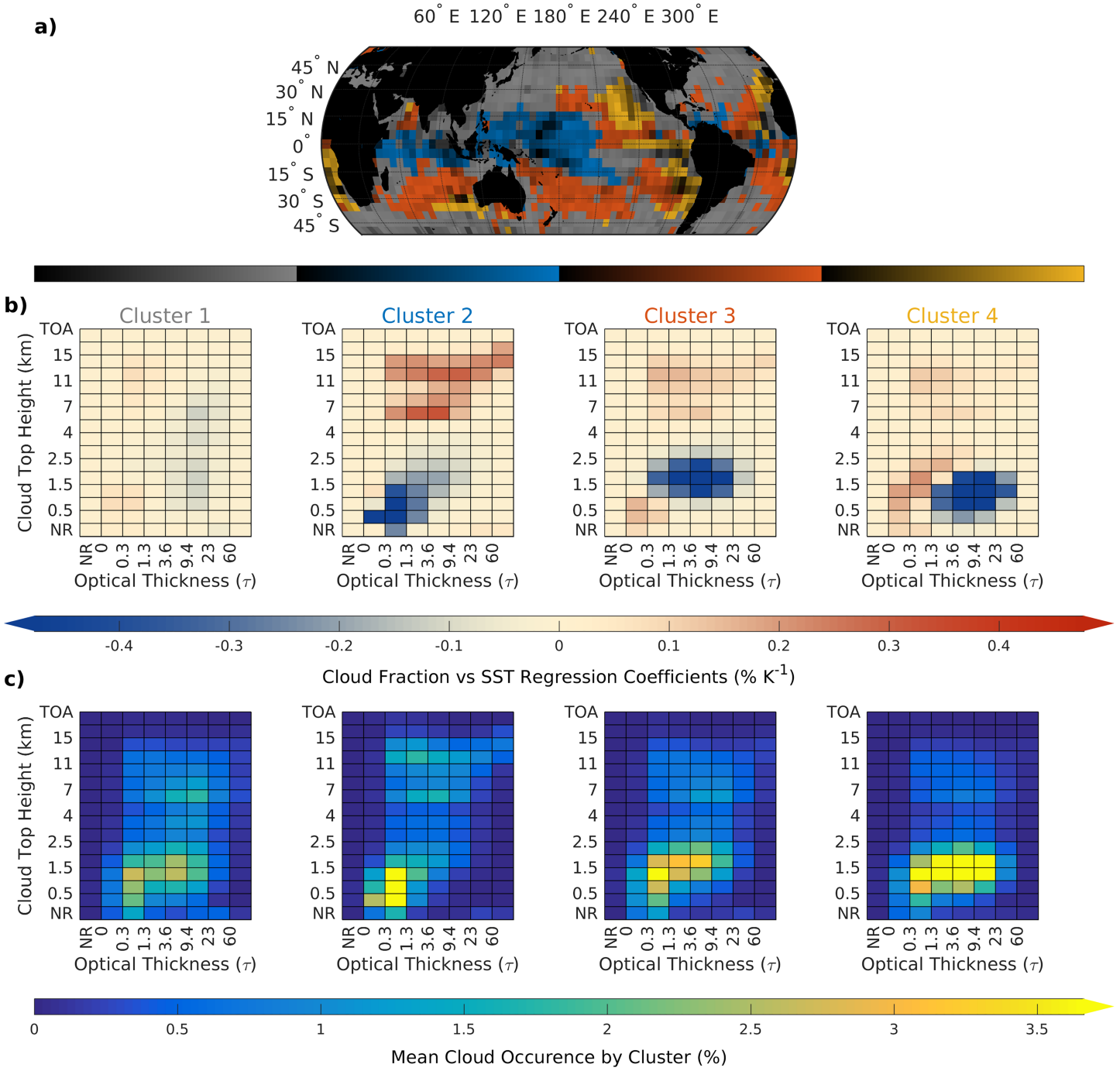


**Figure 2.** Cluster analysis of MISR cloud fraction to SST regression coefficients (2000–2015). Color in panel (a) denotes cluster assignment, and brightness/shading represents the accuracy of the assignment (dimensionless). Row (b) shows four cluster centers computed from SST—cloud fraction regression coefficients. Regression coefficients are computed for each bin in the MISR cloud fraction joint histograms, which sort cloud with respect to cloud top height and optical thickness. Most of the mid-high latitudes show no strong interaction between SST and cloud fraction on monthly timescales (cluster 1). The third and fourth clusters show the well-documented negative correlation between SST and subtropical low cloud. The second cluster likely results from modes of tropical variability (e.g., El Niño) that influence both SST and cloud fraction. For reference, row (c) shows the climatological mean cloud occurrence for each cluster.

values between −3 and $-11\%K^{-1}$ for regions in the Southeast Pacific and Atlantic oceans, Weare (1993) computes values near $-6\%K^{-1}$ for the subtropical stratus regions and $-3\%K^{-1}$ for the subtropics near the center of ocean basins, and Klein and Hartmann (1993) estimate $-5\%K^{-1}$ for the subtropical stratocumulus regions in the East Pacific. Cesana et al. (2019) find $-3.59\%K^{-1}$ in subtropical regions with

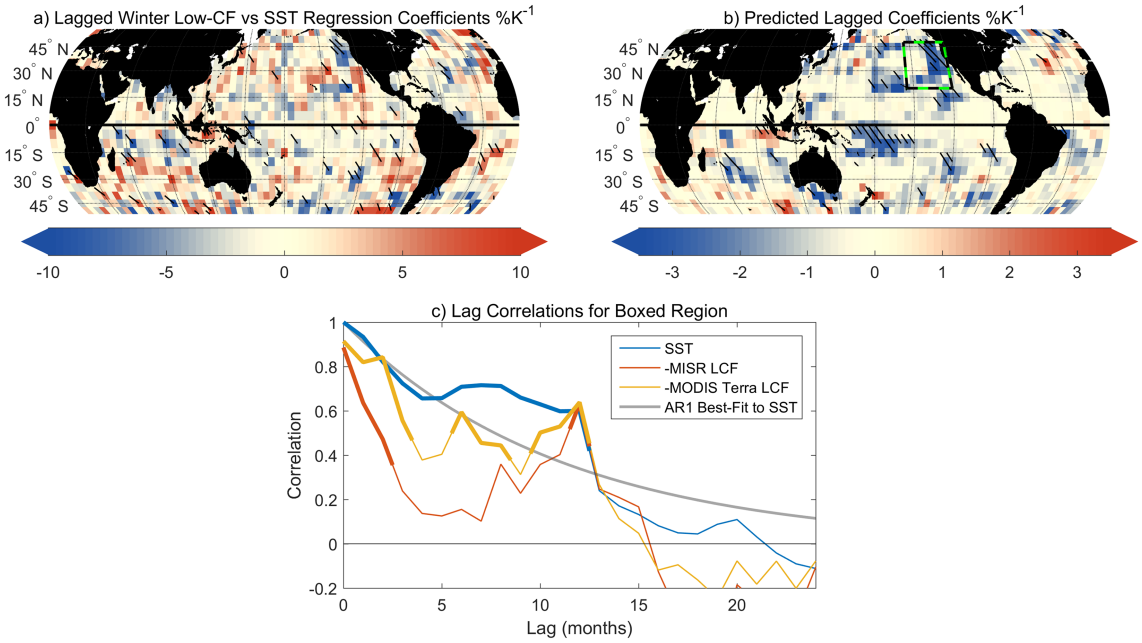


**Figure 3.** (a) Seasonal lag regression between winter/spring SST and winter low cloud fraction (LCF) anomaly the following year (March/October SST vs. February/July LCF in the northern/southern hemispheres). Hatching indicates 95% confidence interval. Panel (b) shows predicted seasonal lag regression coefficients determined by taking the product of SST-SST lag regression coefficients computed over a longer 33-year SST data set and instantaneous wintertime SST-LCF regression coefficients (more analysis in supporting information Section 3). The Northeast Pacific Ocean shows a stronger SST-LCF lagged interaction than other regions. Panel (c) shows lag correlations between March SST and SST and LCF in subsequent months (MISR: CTH < 3 km, MODIS: CTP > 680 hPa) for the boxed region in panel (b). A 3-month boxcar filter has been applied to the data before computing correlations, and the sign of the SST to low cloud-fraction lag correlations is flipped for easier comparison to the SST autocorrelation curve (the true coefficients are negative). The solid gray line is a best fit autocorrelation function for a red-noise process. Bold sections of the curves indicate 95% confidence interval. The deviation from the red-noise autocorrelation function (the hump) around 8- to 12-month lag shows the SST reemergence and associated reduction in low cloud cover.

tropospheric subsidence. Recent studies which estimate the marine stratocumulus response to SST changes as a climate feedback give values around $1.0 \pm 0.7$ $Wm^{-2}$ $K^{-1}$ for the subtropics (Klein et al., 2010). This value is a change in top of atmosphere net shortwave flux due to a 1 K increase in global surface temperature. Assuming a 1 $Wm^{-2}\%^{-1}$ relationship between shortwave radiative flux and subtropical cloud fraction (Klein & Hartmann, 1993), and a 0.7 K change in SST per 1 K surface warming (Klein et al., 2010), this corresponds to a −0.4 to −2.4%K low cloud fraction change due to changes in SST. Hanson (1991) also estimated a weaker relationship of $-1.5\%K^{-1}$. We note that the *k*-means clustering approach has, by design, identified regions with a strong SSTA-CFA relation, and computing a regression between MISR low cloud amount and SST for the entire subtropics (10–30° latitude) gives $-1.7\%K^{-1}$.

### 3.3. Lagged SST-Cloud Fraction Anomaly Comparison

We now use the results in sections 3.1 and 3.2 to guide a global survey of winter/spring SSTA and multi-season lagged total low cloud fraction anomaly (LCFA—defined as cloud with cloud top height below 3 km for MISR and cloud top pressure greater than 680 hPa for MODIS). Lagged SSTA-LCFA regression coefficients (units of $\%K^{-1}$) are shown in Figure 3a, where we compare March SSTA to the subsequent February averaged MISR LCFA for locations in the northern hemisphere and October SSTA to July LCFA in the southern hemisphere, based on the results in section 3.1. These data have been deseasonalized and detrended, and the climatological mean has been subtracted prior to analysis.

The lagged SSTA-LCFA regression coefficients are spatially variable/noisy, and it is difficult to see any coherent patterns. The MISR monthly cloud occurrence data set used here is 15 years long, and because we are showing *seasonal* lag relationships, the regression coefficients in Figure 3a are computed using only 15 observations, and this variability might be expected. We note here that several other longer cloud occurrence data sets exist. In supporting information Section 4 we perform an analysis using the International Satellite Cloud Climatology Project (ISCCP) (Rossow et al., 2016) and Extended Edited Synoptic Cloud

Reports Archive (EECRA) (Hahn et al., 1999) cloud data sets but find that each of these data sets has limitations which restrict their usefulness for this type of seasonal lag correlation analysis. We also attempted to control for the component of the LCF variability that is driven by the free troposphere by performing a similar analysis with EIS computed using ERA Interim reanalysis data (Dee et al., 2011), but this did not substantially alter our results. The OISST data set is 33 years long, however. Thus, while we cannot compute the SSTA-LCFA regression with more than 15 monthly observations, we can compute predictions for these regression coefficients using the historical SST data. We do this by taking the product of SSTA-SSTA seasonally lagged regression coefficients (representing SST reemergence strength in $KK^{-1}$) computed from the 33-year data set, and instantaneous wintertime (December–March and June–September averaged for the northern and southern hemispheres, respectively) SSTA-LCFA regression coefficients (units of $\%K^{-1}$). The product of these two fields (units of $\%K^{-1}$) is a *predicted* response of winter LCFA to the SSTA reemergence mechanism (Figure 3b). This metric highlights the Northeast Pacific region and suggests that here, wintertime SSTA influences wintertime LCFA the following year. In supporting information Section 3 we compute similar predicted correlation coefficients while accounting for the component of the lagged regression coefficients due purely to autocorrelation and not SST reemergence and find that while the large coefficients seen in Figure 3b in the tropics disappear, the Northeast Pacific still shows a strong relationship.

In Figure 3c we examine this Northeast Pacific region in greater detail and show the seasonal lagged correlations for lags between 0 and 24 months between monthly LCFA and SSTA from the preceding March, for values that have been averaged over the box drawn in panel (b) (the sign of the SSTA-LCFA lag correlations is flipped in Figure 3c for easier comparison to the SSTA-SSTA lag correlations). To further reduce the noise, we have applied a 3-month moving average to the LCFA and SSTA time series. All lag correlation functions show an initial reduction over the summer and then an increase the following winter. While SSTA is strongly autocorrelated in this region, the winter-winter SSTA correlation exceeds what is expected from an AR1 process (gray line in Figure 3c), suggesting that in the northeastern Pacific, wintertime low cloud amount is influenced by the previous winter's SSTA.

In summary, in Figure 3a we show the spatial distribution of the relationship between SST reemergence and LCF, but because of the short duration of the data set there is a lot of spatial variability. The statistical model in Figure 3b gives an idea of where we might expect a relationship to exist. Finally, Figure 3c shows lag regressions computed over the region suggested by Figure 3b, and taking the large spatial mean removes much of the noise. While the correlations in Figure 3c do not necessarily imply causation: that SST is determining the shape of the LCF lag correlation function, the physical mechanism for SST reemergence and the linkage between LCF and SST in this region are very well established in the literature. Nonetheless, the analysis itself does not establish that SST and LCF are not responding to some other mechanism. For example, a possible alternative mechanism that we have tested for is the possibility of a strong seasonal dependence in instantaneous LCF-SST correlations. If the SST lag correlation signal were purely red (no reemergence) and there was a strong seasonal dependence in instantaneous LCF-SST correlation (e.g., correlated in the winter but decorrelated in the summer), the winter seasonal SST-LCF lag correlations could appear to have a reemergence signal. However, we do not find a strong seasonal dependence in the instantaneous correlation coefficients between the two data sets, and we can eliminate this alternative. Thus, while it seems very likely that SST reemergence is determining the shape of the LCF seasonal lag correlations, additional modeling studies should perhaps be undertaken to further explore this relationship.

## 4. Discussion and Conclusions

In the introduction we posed the question, does wintertime or early spring SST influence low cloud amount the following winter? The results in section 3.3 indicate that it does in the North East Pacific but has little impact in other areas. So why do we observe this phenomenon only in this region? Figure 1 shows that reemergence is strongest in the mid latitudes, while Figure 2 shows that SST impacts on MSC are strongest in the subtropics and the eastern boundaries of the ocean basins, and these regions have little overlap. Only in the Northeast Pacific do we find a region where SST reemergence extends into the subtropics (Figure 1c) where there is also a strong relationship between SST and low cloud amount (Figure 2a). In other regions we find one, but not both factors: The stratocumulus dominated eastern subtropics of the other ocean

basins have no strong reemergence signal, while the areas with SST reemergence tend to be farther poleward and westward, where there is not a strong SST-LCF correlation.

The atmospheric and ocean variability in the Northeast Pacific are unique: The subtropics are farther from the location of peak cyclogenesis in the western North Pacific than its North Atlantic counterpart, and the Southern Ocean storm tracks are more active than those in the northern hemisphere because they are not obstructed by large continents. Alexander et al. (1999) show that SST reemergence in the Northeast Pacific is particularly strong with a correlation of 0.9 between subsurface temperatures August-September and 0–150 m average temperature in March, consistent with Figure 1. This could be owing to the relatively shallow depth where sequestered temperatures reside, and the relatively weak atmospheric variability in the region. They also found that the correlations are significantly smaller in the Central Pacific. Sugimoto and Hanawa (2005) show that they are weak south of 30°N near 135° because of degradation of the subsurface temperature signal owing to salt fingering.

Subtropical cloud influences Earth's radiative energy budget, and understanding and quantifying the relationship between LCF and SST are important from a climate perspective. Early studies on the LCFA-SSTA relationship proposed a feedback, whereby LCFA influences SSTA by altering the radiative balance at the surface (e.g., Norris & Leovy, 1994; Oreopoulos & Davies, 1993; Weare, 1993); however, most agreed that the short time-scales associated with cloud processes and the relatively long time-scales associated with SST variability meant that SST was primarily driving LCF (see review by Klein et al., 2010). Evan et al. (2012) estimate the forcing on SST due to a change in LCF as only $-0.93\ \mathrm{Wm}^{-2}\%^{-1}$ in the subtropics. More recent work however finds that LCF radiative effects may play a substantial role in maintaining modes of extratropical SST variability, for example, the Atlantic Multidecadal Oscillation (Bellomo et al., 2016, 2013; Myers et al., 2017; Yuan et al., 2016), which suggests perturbations to SST caused by LCF anomalies are important on longer than monthly time scales.

The SST-LCF reemergence mechanism described in this paper means that every winter a predictable change in SST occurs and alters cloud fraction, and this relationship might be used to assess the sensitivity of cloud cover to SST. Averaged over the Northeast Pacific region in Figure 3b, the linear regression between February–April averaged SSTA and January–March averaged LCFA the following year gives a regression coefficient of $-5.5 \pm 7.4\%\mathrm{K}^{-1}$. This is in line with the regressions based on instantaneous values given in section 3.2 and supports the idea that SSTA primarily influences LCFA but has a large 95% confidence interval, which is an unavoidable consequence of having only one sample per year. Thus, while this approach provides some clues regarding the cloud-SST relationship in this region, it will take many decades of reliable data for these estimates to become practical. Furthermore, while the lagged regressions suggest cause and effect (SSTA from the previous spring instigates the change in LCF in the following winter), the regression does not remove the impact of any sub-monthly time-scale positive feedbacks (low cloud fraction altering solar heating of the ocean mixed layer). While the impact of low cloud anomalies on SSTA is likely to be weak, the correlation of winter and spring SST with low cloud cover the subsequent winter provides a potential pathway for cloud cover to have inter-annual and potentially multi-year memory in the Northeast Pacific.

### 4.1. Data sets

Reynolds, R., V. Banzon, and NOAA CDR Program (2008): NOAA Optimum Interpolation 1/4 Degree Daily Sea Surface Temperature (OISST) Analysis, Version 2. 1 December 1981 to 1 August 2016. NOAA National Centers for Environmental Information. doi:10.7289/V5SQ8XB5 Accessed: 13 September 2016.

The MISR CTH-OD data set does not have a DOI. Questions regarding this product can be directed to Roger Marchand (rojmarch@uw.edu).

The MODIS Terra C6 data: https://doi.org/10.5067/MODIS/MYD08_M3.006

**Acknowledgments**
This research was supported by the MISR project at the NASA Jet Propulsion Laboratory (under Contract 1318945), and we wish to acknowledge the many contributions of the MISR team at JPL and the NASA Langley Research Center Atmospheric Science Data Center without whom this project would not have been possible.

## 5. Conflict of Interest

The authors declare that they have no competing interests.

## References

Alexander, M., & Deser, C. (1995). A mechanism for the recurrence of wintertime midlatitude SST anomalies. *Journal of Physical Oceanography*, *25*, 122–137. https://doi.org/10.1175/1520-0485(1995)025<0122:AMFTRO>2.0.CO;2

Alexander, M., Deser, C., & Timlin, M. (1999). The reemergence of SST anomalies in the North Pacific Ocean. *Journal of Climate*, *12*, 2419–2433. https://doi.org/10.1175/1520-0442(1999)012<2419:TROSAI>2.0.CO;2

Alexander, M., Timlin, M., & Scott, J. (2001). Winter-to-winter recurrence of sea surface temperature, salinity and mixed layer depth anomalies. *Progress in Oceanography*, *49*(1-4), 41–61. https://doi.org/10.1016/S0079-6611(01)00015-5

Banzon, V., Smith, T. M., Chin, T. M., Liu, C., & Hankins, W. (2016). A long-term record of blended satellite and in situ sea-surface temperature for climate monitoring, modeling and environmental studies. *Earth System Science Data*, *8*, 165–176. https://doi.org/10.5194/essd-8-165-2016

Bellomo, K., Clement, A., Mauritsen, T., Radel, G., & Stevens, B. (2013). Simulating the role of subtropical stratocumulus clouds in driving Pacific climate variability. *Journal of Climate*, *27*, 5119–5131. https://doi.org/10.1175/JCLI-D-13-00548.1

Bellomo, K., Clement, A., Murphey, L., Polvani, L., & Cane, M. (2016). New observational evidence for a positive cloud feedback that amplifies the Atlantic Multidecadal Oscillation. *Geophysical Research Letters*, *43*, 9852–9859. https://doi.org/10.1002/2016GL069961

Bishop, C. (2006). *Pattern recognition and machine learning*. New York, NY: Springer Science.

Bony, S., & Dufresne, J.-L. (2005). Marine boundary layer clouds at the heart of tropical cloud feedback uncertainties in climate models. *Geophysical Research Letters*, *32*, L20806. https://doi.org/10.1029/2005GL023851

Boucher, O., Randall, D., Artaxo, P., Bretherton, C., Feingold, G., Forster, P., et al. (2013). *Clouds and aerosols, in: Climate change 2013: The physical science basis, contribution of working group I to the fifth assessment report of the intergovernmental panel on climate change* (pp. 571–658). Cambridge, UK and New York, NY: Cambridge University Press. https://doi.org/10.1017/CBO9781107415324

Bretherton, C. (2015). Insights into low-latitude cloud feedbacks from high-resolution models. *Philosophical Transactions of the Royal Society*, *373*, 20140415. http://doi.org/10.1098/rsta.2014.0415

Cesana, G., Del Genio, A. D., Ackerman, A. S., Kelley, M., Elsaesser, G., Fridlind, A. M., et al. (2019). Evaluating models' response of tropical low clouds to SST forcings using CALIPSO observations. *Atmospheric Physics and Chemistry*, *19*, 2813–2832. https://doi.org/10.5194/acp-19-2813-2019

Clement, A., Burgman, R., & Norris, J. (2009). Observational and model evidence for positive low-level cloud feedback. *Science*, *325*(5939), 460–464. https://doi.org/10.1126/science.1171255

Coëtlogon, G., & Frankignoul, C. (2003). The persistence of winter sea surface temperature in the North Atlantic. *Journal of Climate*, *16*, 1364–1377. https://doi.org/10.1175/1520-0442-16.9.1364

Dee, D., & Coauthors (2011). The ERA-Interim reanalysis: Configuration and performance of the data assimilation system. *Quarterly Journal of the Royal Meteorological Society*, *137*, 553–597. https://doi.org/10.1002/qj.828

Diner, D. J., Beckert, J. C., Reilly, T. H., Bruegge, C. J., Conel, J. E., Kahn, R. A., et al. (1998). Multi-angle Imaging Spectroradiometer (MISR) description and experiment overview. *IEEE Transactions on Geoscience and Remote Sensing*, *36*, 1072–1087. https://doi.org/10.1109/36.700992

Eitzen, Z., Xu, K.-M., & Wong, T. (2010). An estimate of low-cloud feedbacks from variations of cloud radiative and physical properties with sea surface temperature on interannual time scales. *Journal of Climate*, *24*(4), 1106–1121. https://doi.org/10.1175/2010JCLI3670.1

Evan, A., Allen, R., Bennartz, R., & Vimont, D. (2012). The modification of sea surface temperature anomaly linear damping time scales by stratocumulus clouds. *Journal of Climate*, *26*(11), 3619–3630. https://doi.org/10.1175/JCLI-D-12-00370.1

Hahn, C. J., Warren, S. G., & Eastman, R. (1999). *Extended edited synoptic cloud reports from ships and land stations over the globe, 1952-2009 (NDP-026C)*. Oak Ridge, TN (United States): Carbon Dioxide Information Analysis Center (CDIAC), Oak Ridge National Laboratory (ORNL). https://doi.org/10.3334/CDIAC/CLI.NDP026C

Hanawa, K., & Sugimoto, S. (2004). 'Reemergence' areas of winter sea surface temperature anomalies in the world's oceans. *Geophysical Research Letters*, *31*, L10303. https://doi.org/10.1029/2004GL019904

Hanson, H. (1991). Marine stratocumulus climatologies. *International Journal of Climatology*, *11*, 147–164. https://doi.org/10.1002/joc.3370110204

Hubanks, P., Platnick, S., King, M., & Ridgway, B. (2015). MODIS atmosphere L3 gridded product algorithm theoretical basis document for C6. http://modis-atmos.gsfc.nasa.gov/_docs/L3_ATBD_C6.pdf

Kara, A., Rochford, P., & Hurlburt, H. (2003). Mixed layer depth variability over the global ocean. *Journal of Geophysical Research*, *108*(C3), 3079. https://doi.org/10.1029/2000JC000736

Klein, S., Hall, A., Norris, R., & Pincus, R. (2010). Low-cloud feedbacks from cloud-controlling factors: A review. *Surveys in Geophysics*, *38*, 1307–1329. https://doi.org/10.1007/s10712-017-9433-3

Klein, S., & Hartmann, D. (1993). The seasonal cycle of low stratiform clouds. *Journal of Climate*, *6*, 1587–1606. https://doi.org/10.1175/1520-0442(1993)006<1587:TSCOLS>2.0.CO;2

Klein, S., Hartmann, D., & Norris, J. (1994). On the relationships among low-cloud structure, sea surface temperature, and atmospheric circulation in the summertime Northeast Pacific. *Journal of Climate*, *8*, 1140–1155. https://doi.org/10.1175/1520-0442(1995)008<1140:OTRALC>2.0.CO;2

Marchand, R. (2012). Spatial correlation of hydrometeor occurrence, reflectivity, and rain rate from CloudSat. *Journal of Geophysical Research*, *117*, D06202. https://doi.org/10.1029/2011JD016678

Marchand, R. (2013). Trends in ISCCP, MISR, and MODIS cloud-top-height and optical-depth histograms. *Journal of Geophysical Research: Atmospheres*, *118*, 1941–1949. https://doi.org/10.1002/jgrd.50207

Marchand, R., Ackerman, T., Smyth, M., & Rossow, W. (2010). A review of cloud top height and optical depth histograms from MISR, ISCCP, and MODIS. *Journal of Geophysical Research*, *115*, D16206. https://doi.org/10.1029/2009JD013422

McCoy, D., Eastman, R., Hartmann, D., & Wood, R. (2017). The change in low cloud cover in a warmed climate inferred from AIRS, MODIS, and ERA-Interim. *Journal of Climate*, *30*, 3609–3620. https://doi.org/10.1175/JCLI-D-15-0734.1

Myers, T., Mechoso, C., & DeFlorio, M. (2017). Coupling between marine boundary layer clouds and summer-to-summer sea surface temperature variability over the North Atlantic and Pacific. *Climate Dynamics*, *50*, 955–969. https://doi.org/10.1007/s00382-017-3651-8

Namias, J., & Born, R. (1970). Temporal coherence in North Pacific sea-surface temperature patterns. *Journal of Geophysical Research*, *75*, 5952–5955. https://doi.org/10.1029/JC075i030p05952

Namias, J., & Born, R. (1974). Further studies of temporal coherence in North Pacific sea surface temperatures. *Journal of Geophysical Research*, *79*, 797–798. https://doi.org/10.1029/JC079i006p00797

Norris, J., & Leovy, C. (1994). Interannual variability in stratiform cloudiness and sea surface temperature. *Journal of Climate*, *7*, 1915–1925. https://doi.org/10.1175/1520-0442(1994)007<1915:IVISCA>2.0.CO;2

Oreopoulos, L., & Davies, R. (1993). Statistical dependence of albedo and cloud cover on sea surface temperature for two tropical marine stratocumulus regions. *Journal of Climate*, *6*, 2434–2447. https://doi.org/10.1175/1520-0442(1993)006<2434:SDOAAC>2.0.CO;2

Peterson, T., Barnett, T., Roeckner, E., & Vonder Haar, T. (1992). An analysis of the relationship between cloud anomalies and sea surface temperature anomalies in a global circulation model. *Journal of Geophysical Research*, *97*, 20497–20506. https://doi.org/10.1029/92JD02282

Rossow, W. B., Walker, A., Golea, V., Knapp, K. R., Young, A., Inamdar A., Hankins, B., & NOAA's Climate Data Record Program (2016). International Satellite Cloud Climatology Project Climate Data Record, H-Series 1-degree monthly, NOAA National Centers for Environmental Information. https://doi.org/10.7289/V5QZ281S

Su, H., & Jiang, J. H. (2013). Tropical clouds and circulation changes during the 2006/07 and 2009/10 El Niños. *Journal of Climate*, *26*, 399–413. https://doi.org/10.1175/JCLI-D-12-00152.1

Sugimoto, S., & Hanawa, K. (2005). Why does reemergence of winter sea surface temperature anomalies not occur in eastern mode water areas? *Geophysical Research Letters*, *32*, L15608. https://doi.org/10.1029/2005GL022968

Timlin, M., Alexander, M., & Deser, C. (2002). On the reemergence of North Atlantic SST anomalies. *Journal of Climate*, *15*(18), 2707–2712. https://doi.org/10.1175/1520-0442(2002)015<2707:OTRONA>2.0.CO;2

Von Storch, H., & Zwiers, F. (2001). *Statistical analysis in climate research*. Cambridge: Cambridge University Press.

Weare, B. (1993). Interrelationships between cloud properties and sea surface temperatures on seasonal and interannual time scales. *Journal of Climate*, *7*, 248–260. https://doi.org/10.1175/1520-0442(1994)007<0248:IBCPAS>2.0.CO;2

Wood, R. (2012). Stratocumulus clouds. *Monthly Weather Review*, *140*(8), 2373–2423. https://doi.org/10.1175/MWR-D-11-00121.1

Wood, R., & Bretherton, C. (2006). On the relationship between stratiform low cloud cover and lower-tropospheric stability. *Journal of Climate*, *19*, 6425–6432. https://doi.org/10.1175/JCLI3988.1

Yuan, T., Oreopoulos, L., Zelinka, M., Yu, H., Norris, J., Chin, M., et al. (2016). Positive low cloud and dust feedbacks amplify tropical North Atlantic Multidecadal Oscillation. *Geophysical Research Letters*, *43*, 1349–1356. https://doi.org/10.1002/2016GL067679

Zhang, Y., Stevens, B., Medeiros, B., & Ghil, M. (2009). Low cloud fraction, lower-tropospheric stability, and large-scale divergence. *Journal of Climate*, *22*(18), 4827–4844. https://doi.org/10.1175/2009JCLI2891.1

Zhao, G., & Di Girolamo, L. (2006). Cloud fraction errors for trade wind cumuli from EOS-Terra instruments. *Geophysical Research Letters*, *33*, L20802. https://doi.org/10.1029/2006GL027088

Zhao, X., & Li, J. (2010). Winter-to-winter recurrence of sea surface temperature anomalies in the northern hemisphere. *Journal of Climate*, *23*(14), 3835–3854. https://doi.org/10.1175/2009JCLI2583.1